Position-sensitive detector

Bodo Kaiser

Ludwig-Maximilians-Universität München

bodo.kaiser@physik.uni-muenchen.de

October 8, 2020

Contents

1. Introduction

We define a position-sensitive device as a device that outputs voltages proportional to the center of mass coordinates of a light beam incident on a sensitive area.

The present document summarizes the insights acquired on the journey of building such a device.

1.1. Motivation

Position-sensitive devices are used in a wide range of industrial and commercial applications, including displacement sensing and beam alignment, see Ref. [7, p. 22].

We are interested in using a position-sensitive device for beam pointing alignment in our quantum optics laboratory.

The beam pointing refers to a laser beam's spatial focus and can change through thermal and mechanical effects. Uncompensated changes in beam alignment can quickly degrade the overall performance of an optical system. Therefore, it is crucial to align the beam pointing to ensure the optical system's proper operation at hand.

1.2. Overview

This document is organized as follows.

The first two sections introduce the theory of the (position-sensitive) photodiode and the operational amplifier. These sections are rather elaborate and should be skipped by the pragmatic scientist.

The third section describes the (electrical) schematics of the detector. If you want to adjust parameters, e.g., gain or bandwidth, you should read these sections.

The fourth section is the only significant section if you want to build a position-sensitive detector (PSD). If you also want an example of using the PSD in an optical setup to determine the spatial resolution, you should also read the fifth section. Finally, the appendix gives some guidance on troubleshooting.

1.3. Requirements

The requirements are specified rather loose. The only hard requirement concerns the connectors and voltages of the power supply. The power connector should be a LEMO4 whose pin configuration is compatible with the 15V dual-voltage power supplies used in the labs. Features that would be nice to have are:

1. The device should be sensible with optical powers that are safe to operate, i.e., P ¡ 1 uW. There is no preferred wavelength.

2. For easy integration into existing optical setups, the device should be as compact as possible. Additional space, if needed, should be occupied by elonging the height. The sensitive area of the detector should be on the bottom. The connectors should be on the top to avoid cables blocking the beam path.

3. It should be possible to mount different detector sizes on the device.

The range of the output voltages of the device can be chosen for the optimal signal-to-noise ratio.

1.4. Specification

2. Position-sensitive photodiode

The present section gives an introduction to the semiconductor theory for a position-sensitive photodiode. We start from the description of a p-n junction and extend the description to the position-sensitive photodiode. After that, we discuss the evolution of position-sensitive photodiode designs. Finally, we derive an analytical relation between the photocurrents and the light focus's position on the sensitive area.

2.1. Transverse photodiodes

The purpose of the following section is to recall the mechanics of the (transverse) photoeffect observed in an illuminated p-n junction. Figures and the description thereof are primarily based on Ref. [11]. A subtle difference in the depicted figures and the figures of Ref. [11] is that we exchanged the order of p- and n-type semiconductors. We found this order to be more intuitive when referring to a p-n junction.
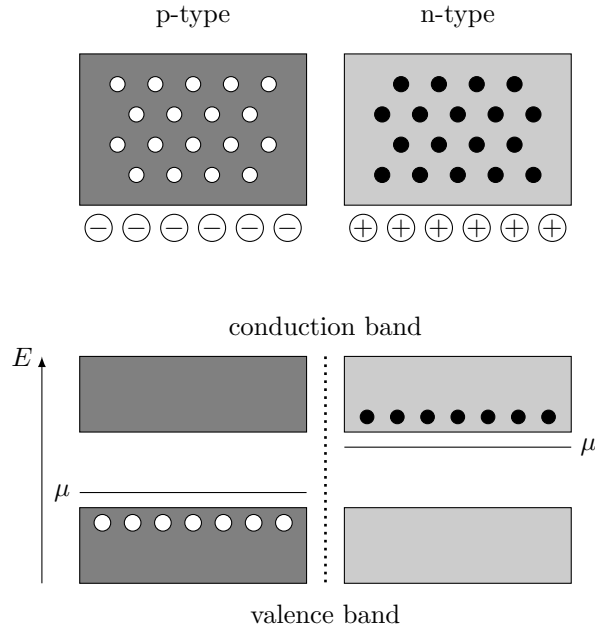

Figure 1: Separated p- and n-type semiconductor with holes (white) and electrons (black).

Figure 1 shows a separated p- and n-type semiconductor. We see an illustration of the p- and n-type semiconductors with their respective mobile charge carriers in the upper half. The p-type semiconductor has an excess of positive charge carriers (holes),

depicted as white circles. The n-type semiconductor has an excess of negative charge carriers (electrons), depicted as black circles. The excess charge carriers form due to the implantation of acceptor and donator ions and are indicated as circles with plus and minus sign in Figure 1. The implanted ions have more or fewer electrons than the atoms of the semiconductor material. Therefore donating an electron or accepting an electron and effectively forming a hole as an absence of negative charge. The lower half of Figure 1 shows the energy band structure of both p- and n-type semiconductors. The lower energy band represents the valence band made up of the tightly bound electrons. The upper energy band represents the conduction band made up of electrons that are are not bound to a single atomic core but shared across the lattice. Charge carriers in the conduction band can move freely and thereby contribute to the conductivity of the material. For an undoped (intrinsic) semiconductor, the chemical potential is in the center of the bandgap between the conduction and valence band. Doping shifts the chemical potential in the p- and n-type semiconductors. In the p-type semiconductor, acceptor ions can take up electrons from the conduction band, thereby decreasing the chemical potential. In the n-type semiconductor, donator ions contribute electrons to the conduction band, increasing the chemical potential.
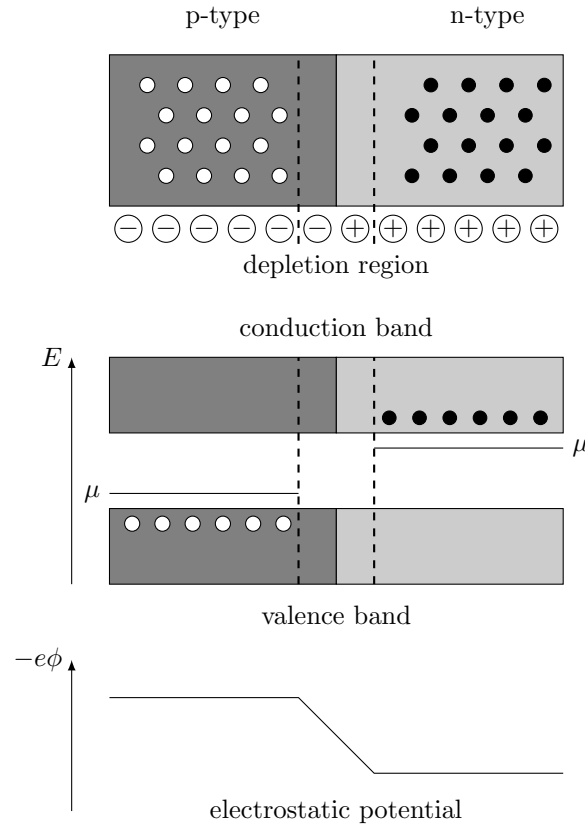

Figure 2: Combined p- and n-type semiconductor with holes (white) and electrons (black).

In Figure 2 the p- and n-type semiconductors are brought into contact with each other, forming a p-n junction. Close to the junction, holes and electrons recombine due to a diffusion process, leaving an electrically charged area. The electrically charged area creates an electrostatic potential across the junction, as illustrated in the lower part of Figure 2. We refer to this area as the depletion region. In Figure 2 the depletion region expands between the dashed lines around the junction.
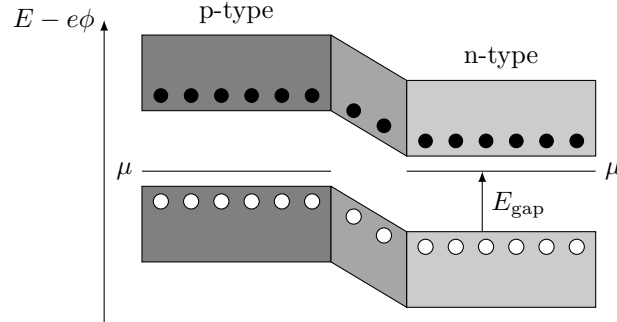
Figure 3: Energy bands of the p-n junction.

The energy band diagram in Figure 3 accounts for the shift in energy due to the electrostatic potential. The chemical potentials of both sides of the junction are now aligned. The energy required to excite an electron on the p-type side from the valence to the conduction band and the energy needed to excite a hole from the conduction to the valence band are equal to the bandgap of the semiconductor. Suppose one applies a reverse bias voltage across the p-n junction. In that case, the effective energy gap between conduction and valence band is reduced, the electrostatic potential increases, and the depletion region broadens. Figure 4 depicts the situation of an applied reverse voltage.

Figure 4: Energy band diagram of a reverse biased p-n junction.

The current-voltage characteristic of the p-n junction is described by the Schockley diode

7

equation,

$$I_{\text{diode}} = I_{\text{sat}}(T) \left(e^{eV/k_B T} - 1 \right), \tag{1}$$
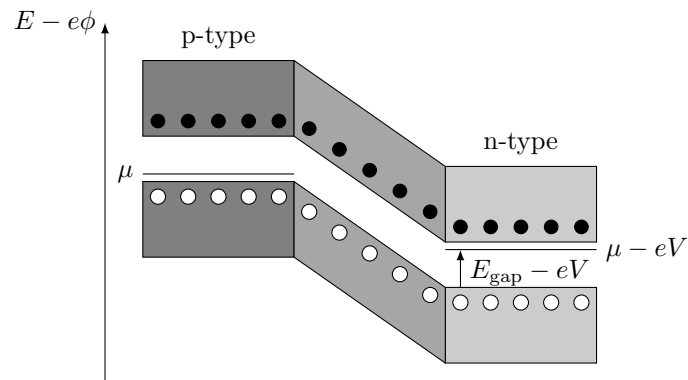
wherein $I_{\text{sat}} \propto e^{-E_{\text{gap}}/k_B T}$ is the temperature dependent reverse bias saturation current and V the voltage applied to the p-n junction. Using the proportionality of the reverse bias saturation current, we can write,

$$I_{\text{diode}} \propto e^{(eV - E_{\text{gap}})/k_B T} - e^{-E_{\text{gap}}/k_B T}, \tag{2}$$

which discloses the two effects contributing to the diode current. The left-hand side of the proportionality of Equation (2) represents the current contribution due to intra-band excitation of charge carriers, whereas the right-hand side represents the current contribution due to inter-band excitation.
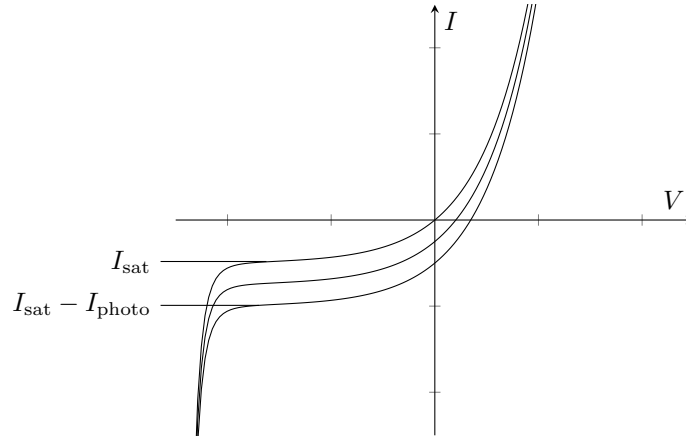
Figure 5: Current-voltage characteristics of a p-n junction with different levels of illumination.

In Figure 5 we see the current-voltage characteristics of the p-n junction under different levels of illumination. For negative voltages, the p-n junction is operated under reverse bias. If the reverse bias voltage exceeds the breakdown voltage, the p-n junction starts to conduct. The reverse saturation current is the amount of current necessary for the breakdown. The curve shifts downwards with increasing illumination. The separation between the non-illuminated (top curve) and illuminated curves represent the respective photocurrent.

The conversion rate of photons to photoelectrons depends on the type of the bandgap, i.e., direct or indirect, the wavelength λ of the photon, and the temperature T. Most photodiodes report a wavelength λ dependent responsivity R which can be used to convert the radiant flux P of the incident light to the generated photocurrent I_{photo},

$$I_{\text{photo}} = R(\lambda)P. \tag{3}$$

For silicon-based p-n junctions, the responsivity $R(\lambda)$ is between $0.2\,\mathrm{A\,W^{-1}}$ at $400\,\mathrm{nm}$ and $0.6\,\mathrm{A\,W^{-1}}$ at $950\,\mathrm{nm}$.
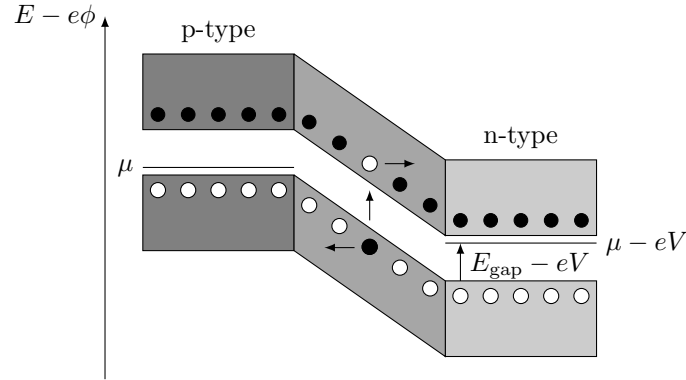
Figure 6: Energy diagram of a reverse biased p-n junction under illumination.

Figure 6 shows a p-n junction under reverse bias where a photon excites an electron-hole pair in the depletion region. Due to the electrostatic potential, the electrons are accelerated to the right. Analogue, the holes are accelerated to the left. The photocurrent, a diode current, Equation (1), flows across the junction.

2.2. Lateral photodiodes

In the previous section, we discussed the transversal photoeffect associated with the p-n junction's illumination. In addition to the transversal photoeffect, the lateral photoeffect was first discovered by W. Schottky [10] in 1930 and later rediscovered in 1957 by J. Wallmark [15]. In the present section, we summarize key results from Ref. [8], and Ref. [17]. The focus of our summary is on the most common position-sensitive photodiode design, the tetralateral photodiode.

Figure 7: Cross section of a lateral photodiode.

Figure 7 depicts the cross-section of a lateral photodiode with a p-type semiconductor as the top, an n-type semiconductor as the middle layer, and a resistive material as the bottom layer. The photodiode's common cathode is an electric contact into the top layer. One can ground or apply a positive voltage to the common cathode. If we apply a positive 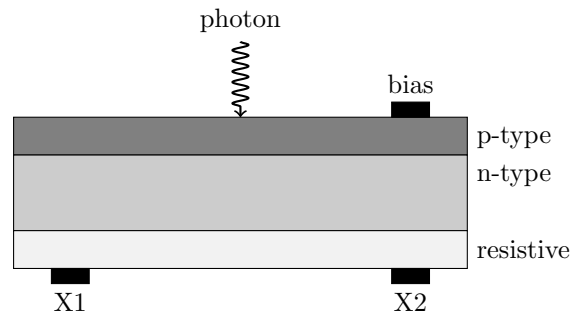voltage, we say that the photodiode is reverse-biased. In contrast to the transversal photodiode, the lateral photodiode has two anode contacts positioned at the opposite sites embedded into the resistive layer. An almost linear relation between the photocurrent at each of the anode contacts and the incident light spot's center-of-mass exists. Therefore the lateral photodiode can be used to measure the spatial coordinate of an incident light spot.

The dynamics of the lateral photodiode are guided by the Lucovsky [14] equation,

$$\nabla^2 V = \frac{\rho}{w} J_s \left(e^{eV/k_B T} - 1 \right) - \frac{\rho_d}{w} J_p, \tag{4}$$

wherein V is the diode voltage, ρ is the resistance per unit length of the resistive layer, J_s is the reverse-bias saturation current and J_p is the photocurrent generated due photon induced electron-hole excitation. Equation (4) can be obtained by a combination of the current density continuity equation with Ohm's law and the Schottky equation, Equation (1).

According to Ref. [17], operation of the lateral in fully reverse-bias has the following benefits:

1. Reduced signal loss.

2. Improved response speed and resolution.

3. Improved linearity of the position.

4. Reduced temperature dependence.

In electronic engineering literature, e.g., Ref. [5, p. 258], one is sometimes discouraged from operating a photodiode under reverse-bias for the highest sensitivity as the reverse-bias increased the diode leakage (dark) current. We believe that as long as the dark current is significantly smaller than the typical photocurrent, the photodiode should always be operated in the reverse-bias mode as recommended by Ref. [8, 17, 16, 4].

Assuming a fully reverse-biased lateral photodiode, we have $eV/k_B T \ll 1$ and Equation (4) simplifies to a linear second order differential (Poisson) equation,

$$\nabla^2 V \approx -\frac{\rho}{w} \left(J_s + J_p \right), \tag{5}$$

which can be solved using variable separation and a product Ansatz. The solution of Equation (5) depends on the imposed boundary conditions. The Dirichlet boundary

condition, $V = 0$, should be used if an electrical contact terminates the semiconductor. Otherwise, the Neumann boundary condition, $\frac{\partial V}{\partial n} = 0$, should be assumed.
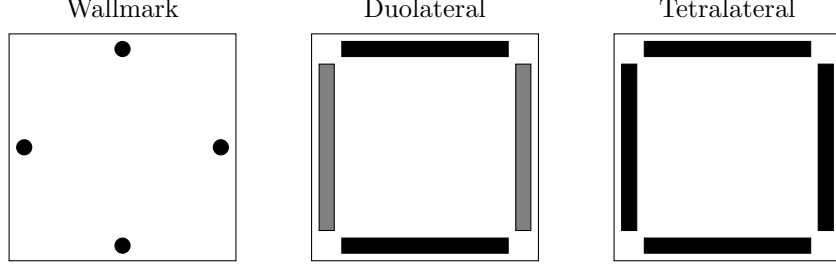

Figure 8: Contact configurations of a lateral photodiode.

In Figure 8 we present three different contact configurations. The left contact configuration, used by Wallmark, comprises four small contacts, see Ref. [15]. Assuming that the contact size is small compared to the photodiode's surface, we need to use the von Neumann boundary condition. The middle contact configuration receives great attention from Noorlag [8]. On two opposite sides of the photodiode, an electric contact terminates the boundary while the remaining sides are left empty. For two-dimensional position detection, one can create two electric contacts at another layer. Mathematically we can express this configuration as a combination of Neumann and Dirichlet boundary conditions. For the tetralateral configuration, we need to apply the Dirichlet boundary conditions for all sides. For a rectangular tetralateral photodiode of width l, the explicit boundary conditions are,

$$V(0, y) = V(l, y) = 0, \qquad\qquad V(x, 0) = V(x, l) = 0. \qquad (6)$$

Together with the initial condition that a focused light spot hits the photodiode at (x^*, y^*),

$$V_p(x, y, t = 0) = I_p \frac{\rho}{w} \delta(x - x^*)\delta(y - y^*), \qquad (7)$$

the general solution of the Lucovsky equation, Equation (5), for the tetralateral configuration reads,

$$V_p^*(x, y) = I_p \frac{\rho}{w} \sum_{n \in \mathbb{Z}} \sum_{m \in \mathbb{Z}} \frac{\sin(m\pi x/l)\sin(m\pi x^*/l)\sin(n\pi y/l)\sin(n\pi y^*/l)}{(m^2 + n^2)\pi^2}. \qquad (8)$$

The current that flows through the $x1$ contact is given by

$$I_{x1}(x^*, y^*) = \frac{w}{\rho} \int_0^l \mathrm{d}y \left. \frac{\partial V}{\partial x} \right|_{x=0}, \qquad (9)$$

respective

$$I_{x1}(x^*, y^*) = \frac{2}{\pi} I_p \sum_{n \in \mathbb{Z}} \frac{\sin[(2n-1)\pi y^*/l]}{2n-1} \frac{\sinh[|2n-1|\pi(1 - x^*/l)]}{\sinh(|2n-1|\pi)}. \qquad (10)$$

11

The solution does not disclose the linear relationship between anode current I_{x1} and the incident spot light coordinate x^*. Ref. [17, Fig. 7] renders the non-linear distortion close to the boundaries as described by Equation (10). In order to show analytically that there is an almost linear relationship between I_{x1} and x^*, we fix $y^* = l/2$, numerically evaluate the dominant terms and Taylor expand the terms to linear order,

$$I_{x1}(x^*, l/2) = \frac{2}{\pi} I_p \sum_{n \in \mathbb{Z}} \frac{(-1)^{n+1}}{2n-1} \frac{\sinh(|2n-1|\pi(1 - x^*/l))}{\sinh(|2n-1|\pi)} \tag{11}$$

$$\approx I_p \left\{ 0.25 - 0.41731 \left(\frac{x}{2l} - 1 \right) \right\} + \mathcal{O}\left(\left(\frac{x^*}{l} - \frac{1}{2} \right)^2 \right). \tag{12}$$

Using the difference between two opposite contacts and normalizing for the total photocurrent, we find,

$$\frac{I_{x2}(x^*, l/2) - I_{x1}(x^*, l/2)}{I_{x1}(x^*, l/2) + I_{x2}(x^*, l/2)} \propto \frac{x}{l}, \tag{13}$$

which indeed is linear in x.

According to Ref. [8, p. 41], the tetralateral photodiode has benefits in manufacturing, although its linearity is below the dual lateral photodiode, still better than the Wallmark type, see Ref. [17]. Recent contact configurations have improved upon the tetralateral design to improve the linearity. For example, the commercially available pin-cushion tetralateral photodiode, discussed in Ref. [2, 16], shows good linearity over a large area. The center-of-mass of an incident light spot at (x^*, y^*) can be recovered from the anode currents via,

$$\frac{(I_{x2} + I_{y1}) - (I_{x1} + I_{y2})}{I_{x1} + I_{x2} + I_{y1} + I_{y2}} = \frac{2x^*}{l} \qquad \frac{(I_{x2} + I_{y2}) - (I_{x1} + I_{y1})}{I_{x1} + I_{x2} + I_{y1} + I_{y2}} = \frac{2y^*}{l}. \tag{14}$$

The datasheet [9] of the S5990, a pin-cushion tetralateral photodiode, discloses the position detectability of a light spot of size $0.2\,\text{mm}$ over a scan interval of $0.4\,\text{mm}$ which does not show any non-linear distortion.

2.3. Equivalent circuit

In the previous section, we described the physics behind the lateral photodiode. In the current section, we want to ignore microscopic details and concentrate on real tetralateral photodiodes' electrical properties.

In Figure 9 the equivalent circuit of a tetralateral photodiode is depicted. The tetralateral photodiode has four anode connections X1, X2, Y1, and Y2 which are connected to the junction via position-dependent resistances R_1, R_2, R_3, and R_4. The actual junction is equivalent to two current sources I_p, I_d, a resistor R_d, and a capacitor C_d in parallel.

The first current source I_p represents the generated photocurrent with typical values between µA and mA. The second current source I_d represents the generated leakage or dark current with typical values between pA and nA.
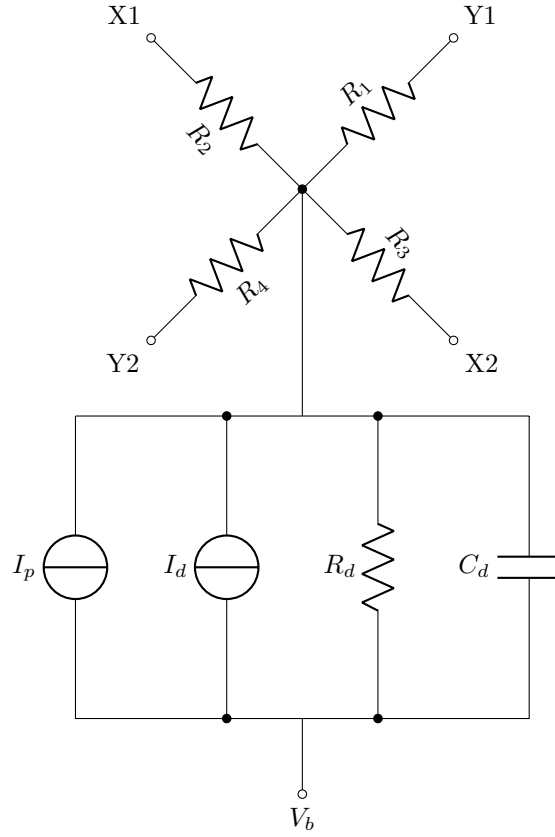
Figure 9: Equivalent circuit of a tetralateral photodiode.

The resistance R_d is referred to as interelectrode resistance and is about $10\,\text{k}\Omega$. The capacitance C_d is also referred to as terminal capacitance and is about $150\,\text{pF}$. Resistance R_d and capacitance C_d form an RC pole which frequency is given by,

$$f_d = \frac{1}{2\pi R_d C_d}. \tag{15}$$

For $R_d = 10\,\text{k}\Omega$ and $C_d = 100\,\text{pF}$ the cut-off frequency f_d of the pole is about $1\,\text{MHz}$, representing the intrinsic bandwidth limit of the detector.

2.4. Signal-to-noise ratio

According to [17], the thermal (Johnson) noise of the resistive component of the lateral photodiode is the dominant noise source. The thermal noise is given by,

$$I_t = \sqrt{\frac{4k_B T B}{R}}, \tag{16}$$

wherein B denotes the bandwidth to consider. At room temperature $T = 300\,\mathrm{K}$ and an interelectrode resistance of $R_d = 10\,\mathrm{k\Omega}$, we find a noise current density due to thermal noise of $i_t = 2\,\mathrm{pA}/\sqrt{\mathrm{Hz}}$. If we estimate for the complete bandwidth supported by the detector, we find a root-mean-squared noise current of $I_t = 2\,\mathrm{nA}$. A more realistic bandwidth incoporating later analog components would be $B = 10\,\mathrm{kHz}$, yielding $I_t = 200\,\mathrm{pA}$.

In any case, we cannot say for sure how these noise sources propagate into position detection noise. For instance, if the noise propagates in the same proportions over the anodes, any error should cancel out when calculating the position.

3. Operational amplifiers

The photocurrents created by our detector are in the range of microampere where they are vulnerable to noise. Using a preamplifier, we can increase the amplitude of the signal for an improved signal-to-noise ratio. The typical photocurrent preamplifier is based on the transimpedance (current-to-voltage) amplifier design using a voltage-feedback operational amplifier. Converting the current signal to a voltage has some benefits. First, an oscilloscope can monitor voltages but not currents. Second, the voltage-feedback operational amplifier is more common than the current-feedback operational amplifier. As a consequence, manufacturers offer a broader product catalog, and there are mentions in the literature. That said, current-feedback operational amplifiers are a viable solution for high-speed and high-bandwidth applications. Read Ref. [5, p. 110] for an overview of the benefits of current-feedback amplifiers, and Ref. [1, Ch. 9] for comparison with voltage-feedback amplifiers. An embodiment of current-feedback operational amplifiers for high-accuracy applications can be found in Ref. [8, p. 143].

In the following, we will always refer to the voltage-feedback operational amplifier if not noted otherwise. Moreover, we expect the reader to be familiar with the foundations of the operational amplifier. Well-written introductions to this topic can be found in [5, Ch. 1] and [1, Ch. 3].

3.1. Basic design

Figure 10 illustrates of a basic transimpedance amplifier design. Ignoring imperfections of the photodiode, we can represent the photodiode as a current source. The non-inverting input of the operational amplifier is connected to the ground. The inverting input is coupled with the output of the operational amplifier via a feedback impedance Z_f.
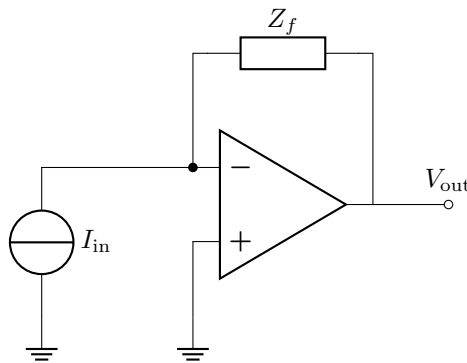

Figure 10: Basic transimpedance amplifier using voltage feedback operational amplifier.

The ideal operation amplifier has zero input current. Thus, in the node of the inverting input of the operational amplifier, Kirchhoff's law states that the current going through the feedback impedance has to cancel the current source I_{in}. The current through the feedback impedance Z_f can be expressed in terms of the feedback impedance Z_f and the output voltage V_{out} of the operational amplifier through the use of Ohm's law, yielding,

$$V_{\text{out}} = -Z_f I_{\text{in}}. \tag{17}$$

Given a maximum current I_{in} and a desired maximum output voltage V_{out}, Equation (17) determines the feedback impedance. Limitations arise for real operational amplifiers where the output voltage is limited to be below the operational amplifier's supply voltage.

Aside from photodiode applications, it is more common to find the inverting (voltage-to-voltage) operational amplifier in the literature. Using the source transformation on the current source with a parallel impedance in the transimpedance amplifier circuit, we can recover the inverting operational amplifier circuit, thereby quickly obtain results for the inverting amplifier configuration.

(a) Transimpedance amplifier.   (b) Inverting amplifier.
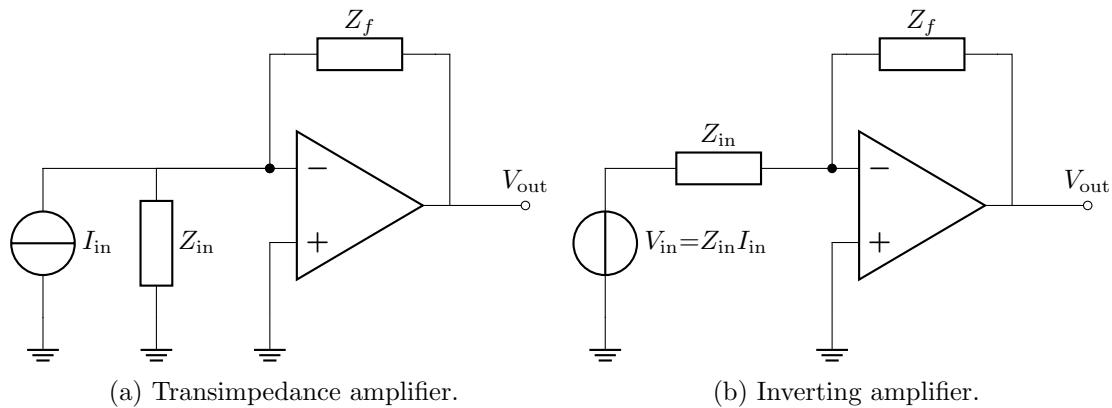
Figure 11: Equivalence between transimpedance and inverting amplifier using source transformation.

Figure 11 shows the source transformation applied to transimpedance and inverting amplifier circuits. Given a current source I_{in} with parallel impedance Z_{in} the equivalent voltage source has value $V_{\text{in}} = Z_{\text{in}} I_{\text{in}}$ with impedance Z_{in} in series.

3.2. Input offset voltage

Real operational amplifiers only reduce the voltage difference between the inverting and non-inverting input to a non-zero input offset voltage. For high-precision operational

amplifiers, the input offset voltage is in the range of microvolts. We can model the input offset voltage as a voltage source at the non-inverting input of an ideal operational amplifier in our transimpedance circuit, as can be seen from Figure 12. In Figure 12 we amended the basic transimpedance circuit of Figure 10 by inserting a voltage source with the input offset voltage between the non-inverting input and ground.
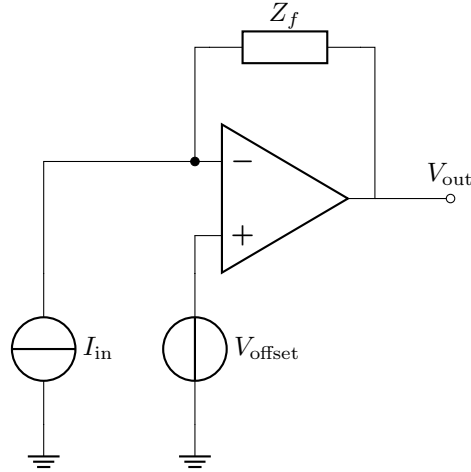
Figure 12: Input offset voltage in the transimpedance amplifier.

We adapt the inverting amplifier's picture to estimate the output offset V_{out} caused by the input offset voltage V_{offset}. Figure 13 shows an inverting amplifier circuit with input impedance Z_{in} and input offset voltage V_{offset} at the non-inverting input of the operational amplifier. According to the superposition theorem, we can replace the input voltage source with a short circuit to estimate the input offset voltage source's contribution.
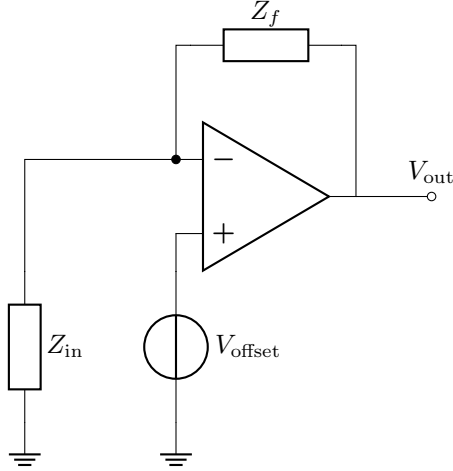
Figure 13: Input offset voltage in the inverting amplifier.

In Figure 13, we identify input and feedback impedance as a voltage divider with exchanged input and output nodes. The respective transfer function reads,

$$V_{\text{out}} = -\frac{R_f + R_{\text{in}}}{R_{\text{in}}} V_{\text{offset}} = -\left(1 + \frac{R_f}{R_{\text{in}}}\right) V_{\text{offset}}. \tag{18}$$

Comparing Equation (18) with Equation (17) discloses a difference in gain. The gain of the input signal in Eq. 1 is commonly referred to as signal gain. The gain of a signal applied directly to the operational amplifier's inputs is referred to as noise gain. In the case of the position-sensitive detector, the input resistance is of order $10\,\text{k}\Omega$. Using a feedback resistance of $R_f = 100\,\text{k}\Omega$, we find that the input offset voltage experiences a gain of 11.

One approach to compensate for the input offset voltage as described is depicted in Figure 14, see also Ref [5, p. 54]. A potentiometer with maximum resistance Rp connects the positive and negative supply voltage. The wiper of the potentiometer is connected with a first resistor R1 to a node. The node is connected with a second resistor R2, and an optional bypass capacitor to ground. Finally, the equivalent input offset voltage source connects the node with the operational amplifier's non-inverting input.

Figure 14: Input offset voltage compensation using adjustable potentiometer.

Let $0 \leq x \geq 1$ be the position of the potentiometer. For $x = 1/2$, the potentiometer's resistance is $R_p/2$ and there is no offset compensation. For $x < 1/2$, the input o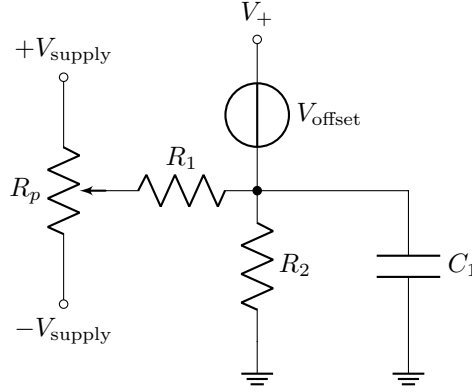ffset compensation is negative to compensate for a positive input offset voltage. For $x > 1/2$, the input offset compensation is positive to compensate for a negative input offset voltage. The maximum input offset compensation is obtained for $x = 0$ and $x = 1$. Using circuit analysis techniques, we obtain,

$$V_c(x) = \frac{R_2(1 - 2x)}{R_1 + R_2 - R_p(1 - x)x} V_{\text{supply}}, \tag{19}$$

as an analytical expression for the input offset voltage compensation measured between the node and ground. The maximum absolute value of the compensation voltage follows to be,

$$V_c(0) = V_c(1) = \pm\frac{R_2}{R_1 + R_2} V_{\text{supply}}. \tag{20}$$

Given a maximum input offset voltage of $100\,\mu\text{V}$ and a supply voltage of $15\,\text{V}$, we find approximate resistor values $R_1 = 3\,\text{M}\Omega$ and $R_2 = 2\,\Omega$. The resistor value of the potentiometer R_p should be sufficiently large to limit the current. For example, a potentiometer resistance of $R_p = 15\,\text{k}\Omega$ would limit the current to $2\,\text{mA}$ with a heat dissipation of $60\,\text{mW}$. In practice, one should aim for a slightly higher maximum compensation voltage to handle resistor mismatches.

That said, there are some practical arguments against the use of the described input offset voltage compensation. The first argument is that the low resistance of R_2 acts as a dominant source for thermal current noise density of about $100\,\text{pA}/\sqrt{\text{Hz}}$. As this current noise contributes to the transimpedance amplifier's input, it gets amplified by the feedback impedance Z_f, yielding up to $110\,\mu\text{V}/\sqrt{\text{Hz}}$ in voltage noise density, which — depending on the bandwidth — surpasses the actual input offset voltage to compensate. The second argument is that high-precision potentiometers with large dynamic range get very large and complicated to accommodate on a printed circuit board.

3.3. Input bias current

In addition to the input offset voltage V_{offset}, there is a second effect that causes an offset in the output voltage V_{out}. This second effect stems from the small amount of current drawn from the inputs of the operational amplifier. We highlighted the input currents in Figure 15 where they are represented by the current flows i_+ and i_- directly pointing into the inputs of the operational amplifier in the transimpedance circuit.
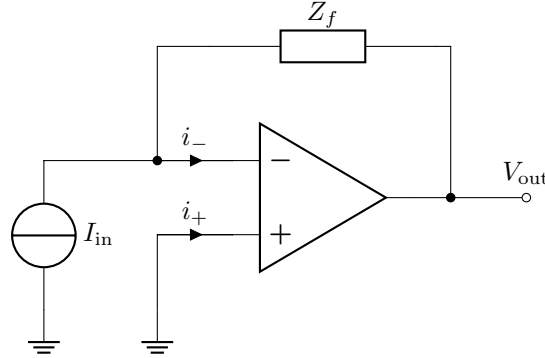
Figure 15: Input bias current offset in the transimpedance amplifier.

Input bias currents for high-precision operational amplifiers are in the range of picoamperes. These small currents are usually difficult to measure and may differ between inputs. The datasheet of the operational amplifier doesn't report the input bias current per terminal. Instead, the mean I_{bias} and the difference between the input currents I_{offset} are specified. The relationship between the mean input bias current I_{bias} and the input offset current I_{offset} for the actual input bias currents i_+, i_- is given below.

$$i_+ = I_{\text{bias}} + \frac{1}{2}I_{\text{offset}} \qquad\qquad I_{\text{offset}} = i_+ - i_- \qquad (21)$$

$$i_- = I_{\text{bias}} - \frac{1}{2}I_{\text{offset}} \qquad\qquad I_{\text{bias}} = \frac{i_+ + i_-}{2} \qquad (22)$$

According to Ref. [5, p. 57] and Ref. [3, p. 25] the effect of the input bias currents i_+, i_- on the output voltage V_{out} can be compensated with an impedance Z_c at the non-inverting input of the operational amplifier. Figure 16 illustrates the inverting amplifier configuration with such a compensation impedance Z_c.
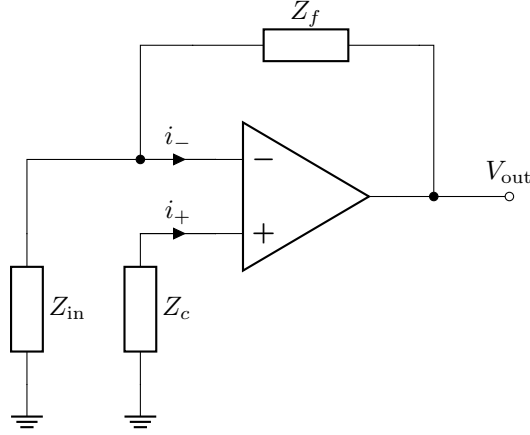
Figure 16: Input current offset compensation.

Following the argumentation from Ref. [12, p. 383], the input bias current at the inverting input of the operational amplifier i_- develops a voltage of $Z_f i_-$ over the feedback impedance Z_f. The input bias current at the non-inverting input i_- develops the voltage $Z_c i_-$ over the compensation resistor Z_c. The voltage $Z_c i_-$ propagates through the voltage divider comprising the feedback and input impedance analog to the input offset voltage. According to the superposition theorem, both of these contributions add and yield,

$$V_{\text{out}} = i_+ Z_c \left(1 + \frac{Z_f}{Z_{\text{in}}} \right) - i_- Z_f, \tag{23}$$

at the output voltage. If $i_+ \approx i_-$ we can choose,

$$Z_c = \frac{Z_{\text{in}}}{Z_{\text{in}} + Z_f}, \tag{24}$$

to compensate for the output voltage offset caused by the input bias currents. The condition $i_+ \approx i_-$ is usually satisfied if the input offset current I_{offset} reported in the datasheet is less than the mean input bias current I_{bias}. High-precision operational amplifiers usually have compensated bias currents that do not satisfy this condition. In this case, there is no generic formula for the value of the compensation impedance Z_c in terms of input and feedback impedance, and one needs to perform impedance matching on a per-device basis. One should keep in mind that high-precision operational amplifiers have input bias currents in the range of pA. Using Equation (23), one should first check if the output voltage offset due to input bias currents is even worth compensating compared to other offset and noise contributions.

3.4. Stability and bandwidth

The outputs of the transimpedance and inverting amplifier designs have a phase shift of 180°. If an additional phase shift of 180° accumulates because of the inherent bandwidth limitations of the operational amplifier and the gain is equal or greater than unity, the conditions for oscillations are met, and the amplifier will become unstable, see Ref. [12, p. 395]. By artificially limiting the bandwidth with an additional frequency pole, we can flatten out the frequency response at high frequencies, and thereby stabilize the amplifier, see Ref. [6, p. 184].

Figure 17 shows a Bode plot of the open-loop (black) and noise gain (red) of an operational amplifier. The noise gain separates into a compensated (solid) and uncompensated (dotted) branch.
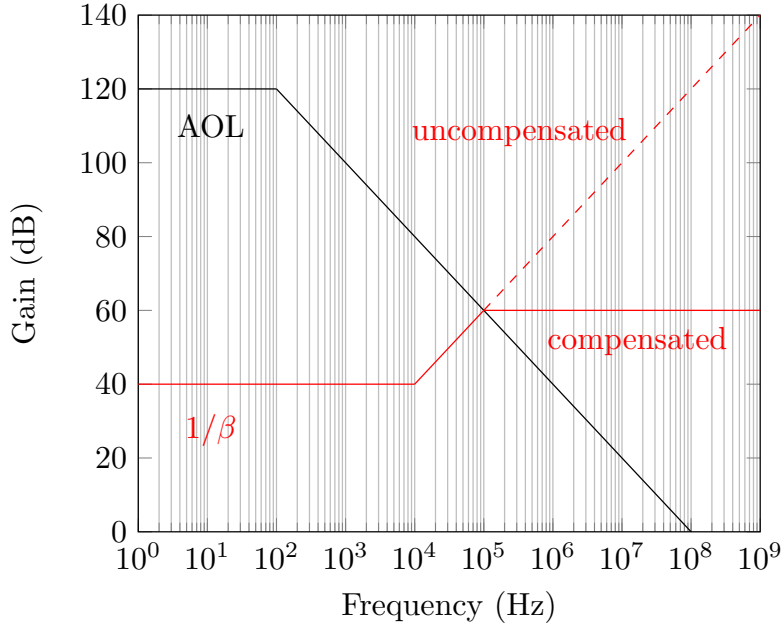
Figure 17: Bode plot of the open-loop and closed-loop gain of the amplifier.

With the uncompensated branch, we would observe instability due to oscillations. Through the addition of a feedback capacitor, we obtain the compensated branch. According to Ref. [5, p. 113], Ref. [4, p. 693] and Ref. [3, Ch. 3] the value for the feedback capacitance is given by,

$$C_f \geq \sqrt{\frac{C_{\mathrm{in}}}{2\pi R_f f_u}}, \tag{25}$$

wherein R_f denotes the feedback resistance and f_u the unity-gain-bandwidth of the op-

erational amplifier. The capacitance should be larger to ensure the design margin. The unity-gain-bandwidth of the operational amplifier denotes the frequency where the open-loop gain equals unity. In the datasheet of the operational amplifier, said frequency is reported as gain-bandwidth-product (GBP). C_{in} in Equation (25) represents the sum of the amplifier circuit's input capacities and the capacitance of the signal source. According to Ref. [1, p. 185] a more exact formula for the feedback capacitance is given by,

$$C_f \geq \frac{C_{\text{aux}}}{2} \left(1 + \sqrt{1 + \frac{4C_{\text{in}}}{C_{\text{aux}}}} \right) \qquad C_{\text{aux}} = \frac{1}{2\pi R_f f_u}, \qquad (26)$$

which is also valid if not $C_{\text{in}} \gg C_f$.

Figure 18 illustrates the transimpedance amplifier with capacitive elements. Parallel to the current source I_{in}, we find the input capacitance C_{in} comprising source capacitance and operational amplifier capacitance. Parallel to the feedback resistance R_f we find the feedback capacitance C_f with value given in Equation (26) or Equation (25).
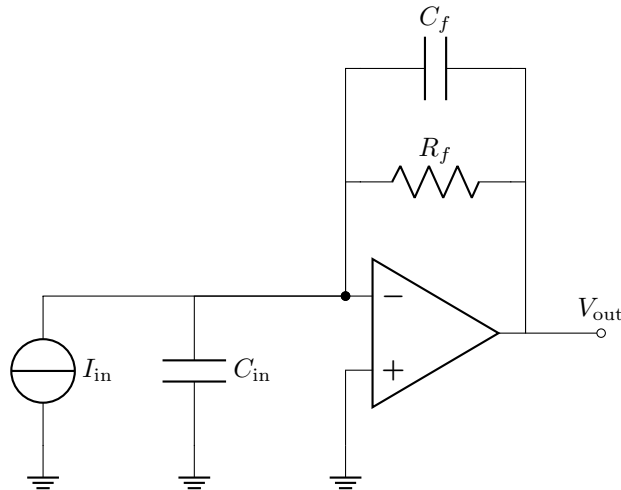
Figure 18: Transimpedance amplifier with capacitive elements.

As noted earlier, the bandwidth reduces with an additional feedback capacitor. The new bandwidth is now given by the RC pole formed by the feedback impedance

$$BW = \frac{1}{2\pi R_f C_f}. \qquad (27)$$

Given a unity-gain-bandwidth of the operational amplifier of $f_u = 10\,\text{MHz}$ and a feedback resistance of $R_f = 100\,\text{k}\Omega$ Equation (25) yields a minimum feedback capacitance of $C_f = 4\,\text{pF}$. Together with R_f, the feedback capacitance limits the bandwidth to about $400\,\text{kHz}$.

23

4. Schematic

The present section discusses the critical sections of the electrical schematics and should be consulted for reference if parameters, for example, bandwidth or gain, need to be adjusted.

4.1. Photodiode frontend

The photodiode frontend is responsible for converting the photocurrent to a voltage. The most simple frontend, a resistor, has limited bandwidth. Using a transimpedance amplifier, we can decouple the output voltage from the voltage swing across the diode. The bandwidth is now limited by the amplifier gain.
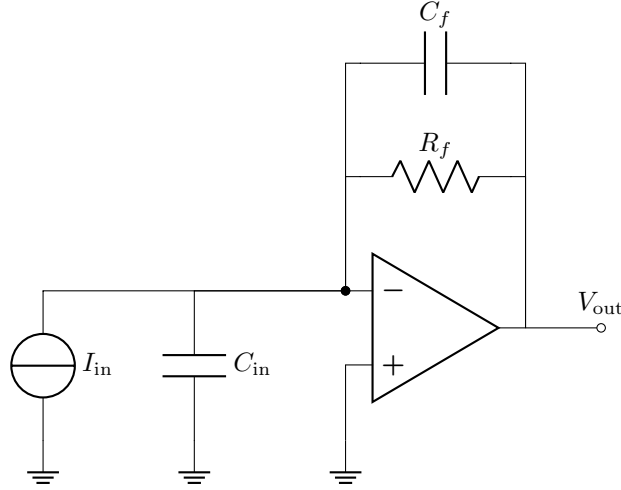
Figure 19: Transimpedance amplifier for photodiode

Figure 19 shows a transimpedance amplifier frontend circuit representing the photodiode by a current source with capacitance. The current source relates to the power of the incident light by

$$I_\mathrm{in} = S(\lambda)P, \tag{28}$$

wherein $S(\lambda)$ is the spectral responsivity, also known as photosensitivity, and P is the power of the light beam.

A class 2 laser can be operated without safety googles. For a Class 2 laser, the beam power is limited to $P \leq 1\,\mathrm{mW}$. With $S = 0.6\,\mathrm{A\,W^{-1}}$, the photocurrent is limited to $I_\mathrm{in} \leq 0.6\,\mathrm{mA}$.

The operational amplifier's output voltage in the transimpedance configuration is equal to

$$V_{\text{out}} = -R_f I_{\text{in}}. \tag{29}$$

The operational amplifier's output voltage is determined by it's supply voltages. For a rail-to-rail operational amplifier it is equal to the supply voltage. For example, if the supply voltage is $\pm 5\,\text{V}$, eq. (29) gives us a value for the feedback resistance,

$$R_f \geq \left| \frac{V_{\text{out}}}{I_{\text{in}}} \right| = \left| \frac{V_{\text{supply}}}{I_{\text{in}}} \right|. \tag{30}$$

Using the previous estimated photocurrent of a class 2 laser, $I_{\text{in}} = 0.6\,\text{mA}$, $V_{\text{supply}} = \pm 5\,\text{V}$, and eq. (30), we find that $R_f \approx 9\,\text{k}\Omega$ would make our transimpedance amplifier saturate at the maximal expected light power.

A feedback capacitance

$$C_f \geq \sqrt{\frac{C_{\text{in}}}{2\pi R_f f_u}}, \tag{31}$$

wherein f_u is the GBP of the operational amplifier, is sufficient for stability. In general, the input capacitance of the operational amplifier adds to the input capacitance. In practice, solder joints and printed circuit board (PCB) traces may add to the capacitance such that a slightly higher value than given by eq. (31) is recommended. However, if the feedback capacitance is too high, we remove high-frequency components of our signal, which might be of interest.

The photodiode's datasheet specifies the capacitance C_{in} to be about $90\,\text{pF}$ if reverse-biased at $10\,\text{V}$. The differential- and common-mode input capacitance of the OPA847 operational amplifier add up to a total input capacitance of $98\,\text{pF}$. Using $R_f = 10\,\text{k}\Omega$ and GBP of $f_u = 10\,\text{MHz}$, a feedback capacitance of at least $C_f = 12.5\,\text{pF}$ should be choosen.

4.2. Voltage regulator

We use two voltage regulators to maintain a constant voltage of $\pm 12\,\text{V}$ from the external $\pm 15\,\text{V}$ power supply. The $\pm 12\,\text{V}$ voltage powers most components except the transimpedance amplifiers of the detector. Using a dedicated pair of voltage regulators to power the transimpedance amplifiers decreases the load on the primary voltage regulator.

Figure 20 shows the circuitry of the primary voltage regulators that output $\pm 12\,\text{V}$. The positive voltage regulator U1 of type LM317 and the negative voltage regulator U2 of type LM337 have an internal reference voltage of $1.25\,\text{V}$.
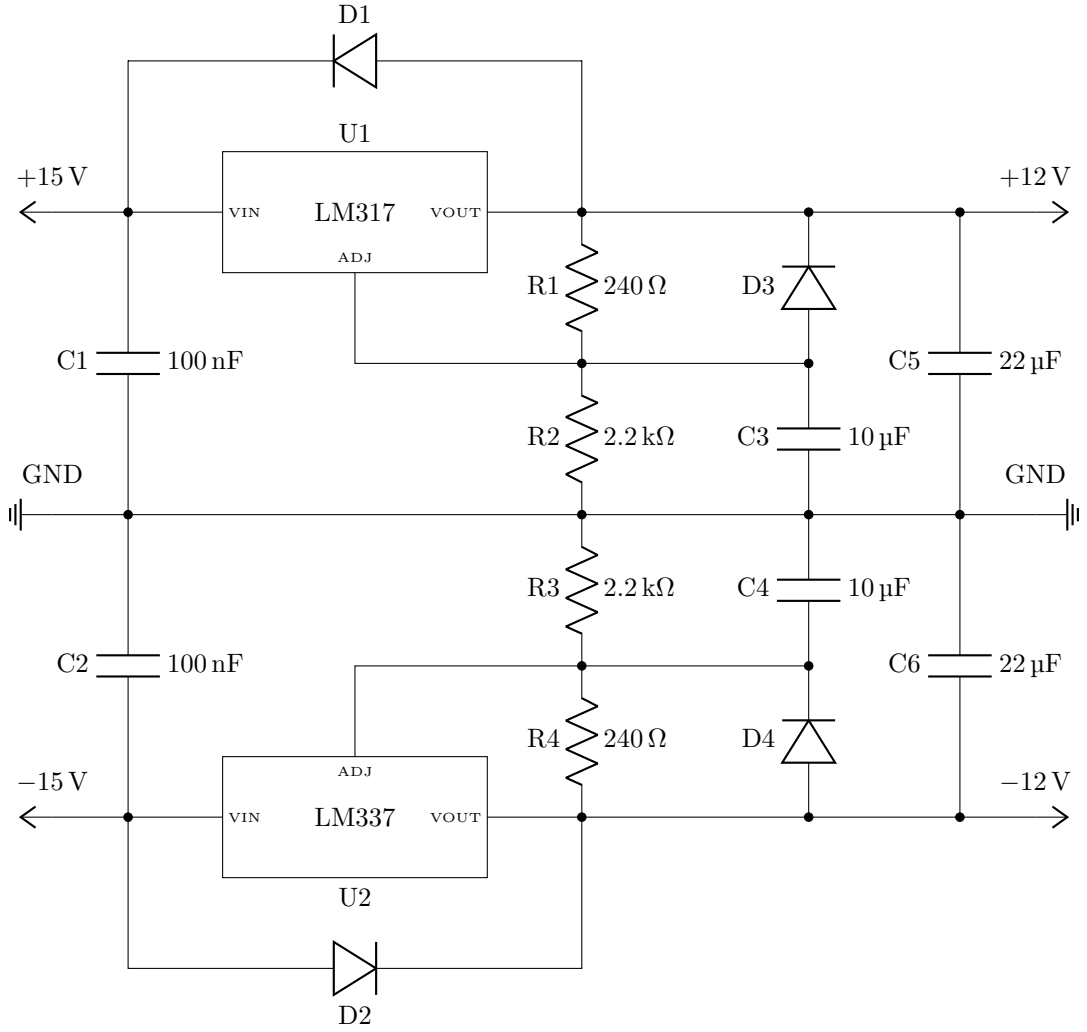
Figure 20: Dual supply voltage regulator

The voltage divider comprising R1 and R2 fixes the output voltage according to

$$V_{\text{out}} = 1.25\,\text{V} \left(1 + \frac{R_2}{R_1} \right). \tag{32}$$

With $R1 = 240\,\Omega$ and $R2 = 2.2\,\text{k}\Omega$, the output voltage is about 12.7 V, which leaves enough space for potential voltage drops in, for example, the operational amplifiers.

Diodes D1 and D3 ensure that the capacitors C3 and C5 can discharge over the external power supply.

The application notes of one of the voltage regulator's datasheets describe the presented

design. That is also the reason for not using fixed voltage regulators in this case.

4.3. Voltage reference

Reverse biasing the photodiode decreases it's capacitance and thereby increases the bandwidth. The reverse bias voltage needs to be well controlled not to cause any side-effects. Therefore, we utilize a voltage reference to supply a highly-regulated reverse voltage for the photodiode.
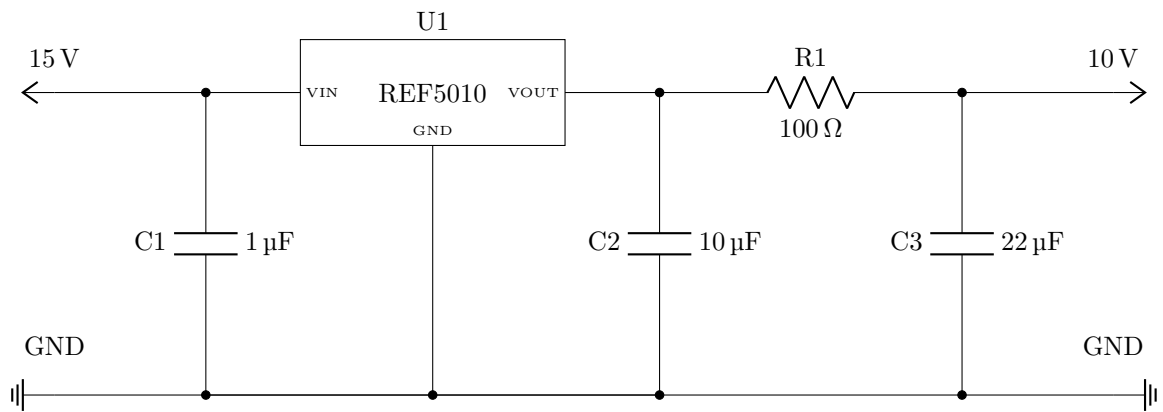
Figure 21: Voltage reference to reverse bias the photodiode

Figure 21 shows the schematic of the reverse-bias voltage reference. The capacitors C1 and C3 intercept voltage fluctuations. Resistor R1 forms a low-pass with capacitor C2 that suppresses frequencies above 160 Hz.

4.4. Analog arithmetic

Finally, we need to add and subtract the four different voltage signals of the position-sensitive photodiode to obtain quantities proportional to the incident light beam's center-of-mass. We achieve immutability of the input signals for addition and subtraction with the summing amplifier. We extend the summing amplifier to allow negative signs, i.e., subtraction.
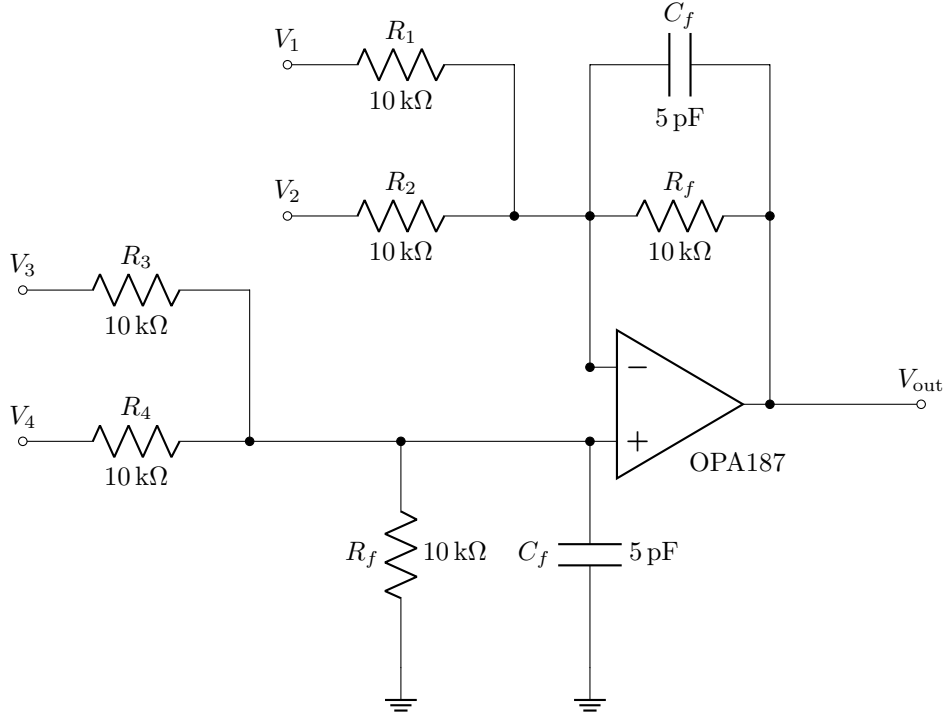
Figure 22: Summing and difference amplifier

Figure 22 shows such an arithmetic amplifier. According to [13, p. 5] the output voltage is given by

$$V_{\text{out}} = -\frac{R_1}{R_f}V_1 - \frac{R_2}{R_f}V_2 + \frac{R_3}{R_f}V_3 + \frac{R_4}{R_f}V_4. \tag{33}$$

It is an excellent directive to have a well-controlled the bandwidth. On this account, we include capacitor C_f to control the frequency response of the amplifier. For the resistor and capacitor configuration used in fig. 22, the bandwidth is equal to

$$\frac{1}{2\pi R_f C_f} \approx 3\,\text{MHz}, \tag{34}$$

magnitudes more than the bandwidth of our transimpedance amplifiers. We place an additional capacitor with feedback capacitance at the non-inverting input of the operational amplifier to obtain a symmetric frequency response for the positive terms in eq. (33).

The value of the resistors is $10\,\text{k}\Omega$ to limit the current flow.

5. Production

The production of the position-sensitive device involves the necessary steps to produce the detector and arithmetic PCB.

It's best to first do the arithmetic board and if it works, proceed with the detector. Of course, if you only need one of the boards, perform the following steps only once.

5.1. Commissioning

Before we can assemble the PCBs, we need to gather the required components and order missing pieces.

The list of the required components is usually known as the bill of materials (BOM). You can generate a current BOM directly from KiCad by using the InteractiveHtmlBom plugin. The plugin generates an hypertext markup language (HTML) file that lists the components and their respective placement on the PCB. Figure 23 shows where to find the plugin in the PCB editor menu. You can check if the parts are stocked and placed.

Figure 23: Menu entry for the InteraciveHtmlBom plugin for KiCad

Figure 24 and fig. 25 show the view of the generated HTML for the arithmetic and detector board.

#	Sourced	Placed	References	Value	Footprint	Quantity
1	☐	☐	C1, C2, C11, C12, C15, C16, C17, C18	100n	C_0603_1608Metric	8
2	☐	☐	C7, C8, C9, C10, C13, C14	5p	C_0603_1608Metric	6
3	☐	☐	C3, C4	10u	C_1210_3225Metric	2
4	☐	☐	C5, C6	22u	C_1210_3225Metric	2
5	☐	☐	R6, R7, R8, R9, R10, R12, R13, R14, R15, R16, R17, R18, R19, R20, R21, R22, R24	10k	R_0603_1608Metric	17
6	☐	☐	R23	2k	R_0603_1608Metric	1
7	☐	☐	R1, R4	240	R_1210_3225Metric	2
8	☐	☐	R2, R3	2.2k	R_1210_3225Metric	2
9	☐	☐	R5	510	R_1210_3225Metric	1
10	☐	☐	R11	470	R_1210_3225Metric	1
11	☐	☐	D1, D2, D3, D4	1N4148	D_SOD-123	4
12	☐	☐	D5, D6	LED	LED_0603_1608Metric	2
13	☐	☐	U3, U4, U5	OPA197xD	SOIC-8_3.9x4.9mm_P1.27mm	3
14	☐	☐	U1	LM317	SOT-223-3_TabPin2	1
15	☐	☐	U2	LM337	SOT-223-3_TabPin2	1
16	☐	☐	G***	LOGO	mpq_lmu_logo	1
17	☐	☐	J1	Conn_01x03_Male	FanPinHeader_1x03_P2.54mm_Vertical	1
18	☐	☐	J2, J3	Conn_01x05_Male	PinHeader_1x05_P2.54mm_Vertical	2
19	☐	☐	J4, J5, J6	Conn_Coaxial	SMA_Molex_73251-2120_EdgeMount	3

Figure 24: Arithmetic board view of the InteraciveHtmlBom plugin

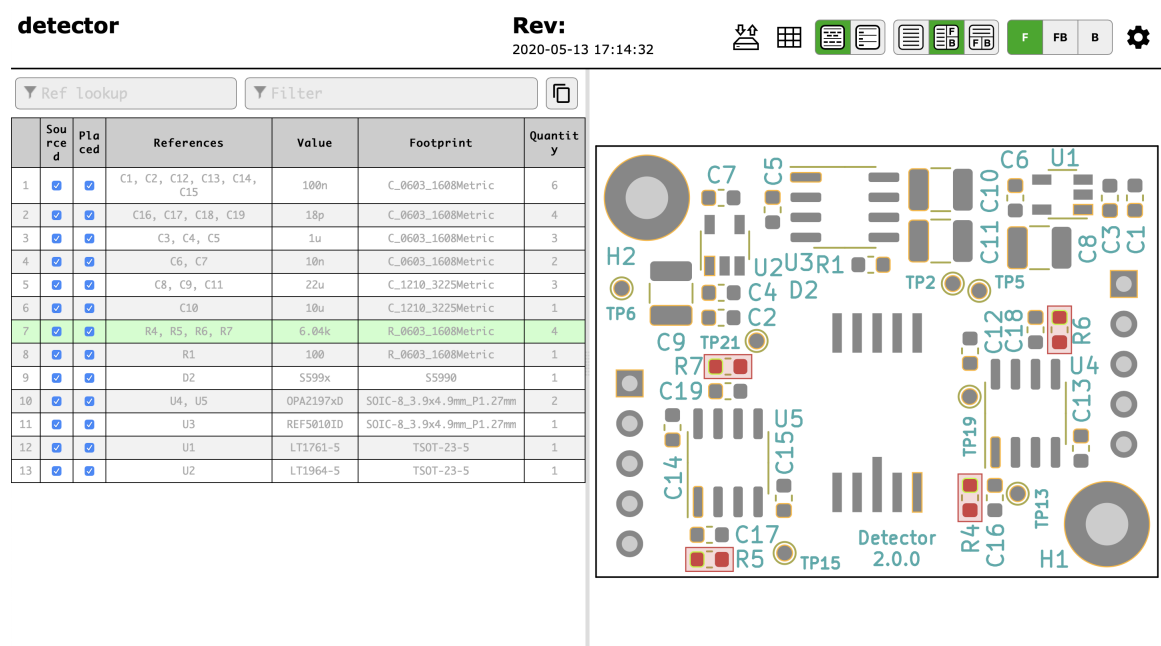| #	Sourced	Placed	References	Value	Footprint	Quantity
1	☑	☑	C1, C2, C12, C13, C14, C15	100n	C_0603_1608Metric	6
2	☑	☑	C16, C17, C18, C19	18p	C_0603_1608Metric	4
3	☑	☑	C3, C4, C5	1u	C_0603_1608Metric	3
4	☑	☑	C6, C7	10n	C_0603_1608Metric	2
5	☑	☑	C8, C9, C11	22u	C_1210_3225Metric	3
6	☑	☑	C10	10u	C_1210_3225Metric	1
7	☑	☑	R4, R5, R6, R7	6.04k	R_0603_1608Metric	4
8	☑	☑	R1	100	R_0603_1608Metric	1
9	☑	☑	D2	S599x	S5990	1
10	☑	☑	U4, U5	OPA2197xD	SOIC-8_3.9x4.9mm_P1.27mm	2
11	☑	☑	U3	REF5010ID	SOIC-8_3.9x4.9mm_P1.27mm	1
12	☑	☑	U1	LT1761-5	TSOT-23-5	1
13	☑	☑	U2	LT1964-5	TSOT-23-5	1

Figure 25: Detector board view of the InteraciveHtmlBom plugin

Start by checking the local inventory for the components listed by the generated HTML

BOM. If certain elements are missing, you can check the `BOM.xlsx` file inside the project repository. It contains part numbers and product links from major electronic distributors. If you order, double-check with the generated HTML BOM. There might be errors, e.g., wrong casing sizes in the `BOM.xlsx` as it is potentially outdated.

5.2. Manufacturing

In the manufacturing process, we solder the components onto the PCB. We recommend to proceed in the following steps:

1. Put on rubber gloves as the solder paste is potentially hazardous.

2. Take out the solder paste from the fridge and let it reach room temperature[1].

3. Place the solder paste onto the contacts of the PCB[2].

4. Place the surface mounted device (SMD) components onto the solder with a tweezer[3].

5. Start the oven and adjust the frame on which you place the board with the screw to the appropriate size. Use an empty PCB for this.

6. Select the profile SMD180 and follow the instructions of the oven.

7. Inspect the board for misplaced components and unmelted solder, and fix them by hand soldering[4].

8. Perform electrical testing as described in the next section.

9. Solder remaining components, for example, the SubMiniature version A (SMA) mounts or the pin headers, by hand.

---

[1]It is possible to use the cold solder paste directly, but it makes the handling more difficult as the paste is less fluid.

[2]Generally speaking, it is better to have too much solder paste then too less. If there is a small overlap between the contacts, this is fine as the solder will shrink when transitioning to a liquid phase in the oven.

[3]Start with the larger components and then progress to the smaller ones

[4]You can use the solder heat gun to melt the remaining solder paste or remove misplaced components. However, you might blow away small capacitors.

5.3. Electrical testing

With the electrical testing, we want to confirm that the solder connections and components work as expected. The most basic check is that the supply voltages are correct. More elaborated checks concern the operational amplifiers but are out of the scope of this document.

For the arithmetic perform the following checks in the given order. Skipping steps might lead to permanent damage!

- ☐ Leave the arithmetic board unpowered and check for high resistance between the supply lines through the test points TP1 ($12\,\mathrm{V}$), TP2 (GND), and TP3 ($-12\,\mathrm{V}$)[5].

- ☐ Configure the power supply to provide a dual voltage of $\pm15\,\mathrm{V}$[6]. If possible, limit the current of the voltage sources.

- ☐ Confirm that the output voltages are correct with the multimeter.

- ☐ Connect the power supply with the arithmetic board but double-check the polarity.

- ☐ The voltage between TP2 and TP1 should read around $12\,\mathrm{V}$ while the voltage between TP2 and TP3 should read about $-12\,\mathrm{V}$.

- ☐ Confirm that the supply voltages reach the op-amps.

- ☐ Check the temperature of the integrated circuit (IC)s. If any IC is very hot, there is a short.

- ☐ Check if the op-amps work by grounding the inverting input and confirming that the output voltage changes to $0\,\mathrm{V}$.

For the detector perform the following checks in the given order. Skipping steps might lead to permanent damage!

- ☐ Leave the detector board unplugged and confirm high resistance between GND (you can use the middle pin of the headers), TP5 ($5\,\mathrm{V}$), and TP6 ($-5\,\mathrm{V}$).

- ☐ Confirm a change of the voltage between the photodiode and GND's outer pins while illuminating the sensitive area of the photodiode with a laser pointer.

---

[5]If there is low resistance ($> 10\,\mathrm{k\Omega}$), you probably have a short through soldering.

[6]Alternatively, use two single voltage sources set to $15\,\mathrm{V}$ and connect the negative port of one of the voltage sources with the other one's positive voltage.

☐ Mount the detector board on the arithmetic board, and measure the detector board's supply voltages.

☐ Confirm that the voltage reference (U3) outputs $10\,\mathrm{V}$ and that the op-amps have the correct supply voltage of $\pm 5\,\mathrm{V}$.

Finally, we test the arithmetic amplifiers on the arithmetic board.

☐ Mount the detector onto the arithmetic board.

☐ Measure the voltage at the outputs of the operational amplifiers of the arithmetic board. For the summing amplifier (U5), we expect an increase in voltage when illuminating the photodiode with the laser pointer. For the difference amplifiers (U3, U4), we expect the voltage to change when moving the laser pointer's focal spot on the photodiode.

6. Measurement

In the present section, we will perform some measurements with the PSD. In particular, we want to determine the spatial resolution and discuss the noise characteristics.

6.1. Electrical setup

Table 1 lists the equipment required for the electrical setup. The electric devices are connected as follows. The PSD is connected with the power supply through the LEMO4 cable. The DIFFX, DIFFY, and SUM output voltages of the PSD are conencted to the oscilloscope's first three input channels. It is essential to use shielded cables to avoid receiving 50 Hz noise from surroudning switching power supplies.

Device	Amount
PSD	1
Oscilloscope	1
$\pm 15\,$V voltage supply	1
Shielded LEMO4 cable	1
Shielded SMA cable	3
SMA to BNC adapters	3

Table 1: Electrical equipment required to operate the PSD

You can configure the oscilloscope to show the first two input channels in X-Y mode. In X-Y mode, the signal on the coordinate grid corresponds to the position of the incident light spot. Suppose your light source shows strong intensity fluctuations. In that case, you can use the oscilloscope's arithmetic operation to divide the DIFFX and DIFFY signals by the SUM signal.

6.2. Optical setup

Figure 26 shows an optical setup for spatial resolution measurements. The arrangement comprises a laser source, two mirrors, a lens with focal length $f = 50\,$mm positioned in 11 cm distance from the PSD. Using two mirrors instead of one allows more freedom in positioning the other optics. The lens focuses the laser beam onto the sensitive area of the PSD. We measured an optical power of $P = 1\,$mW for the red laser at $\lambda = 700\,$nm with the optical power meter.
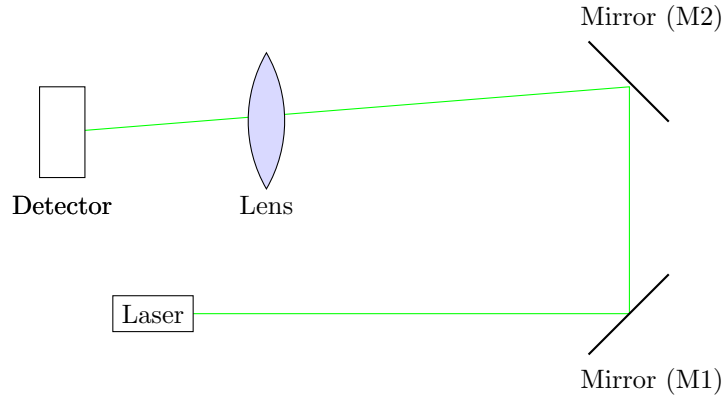
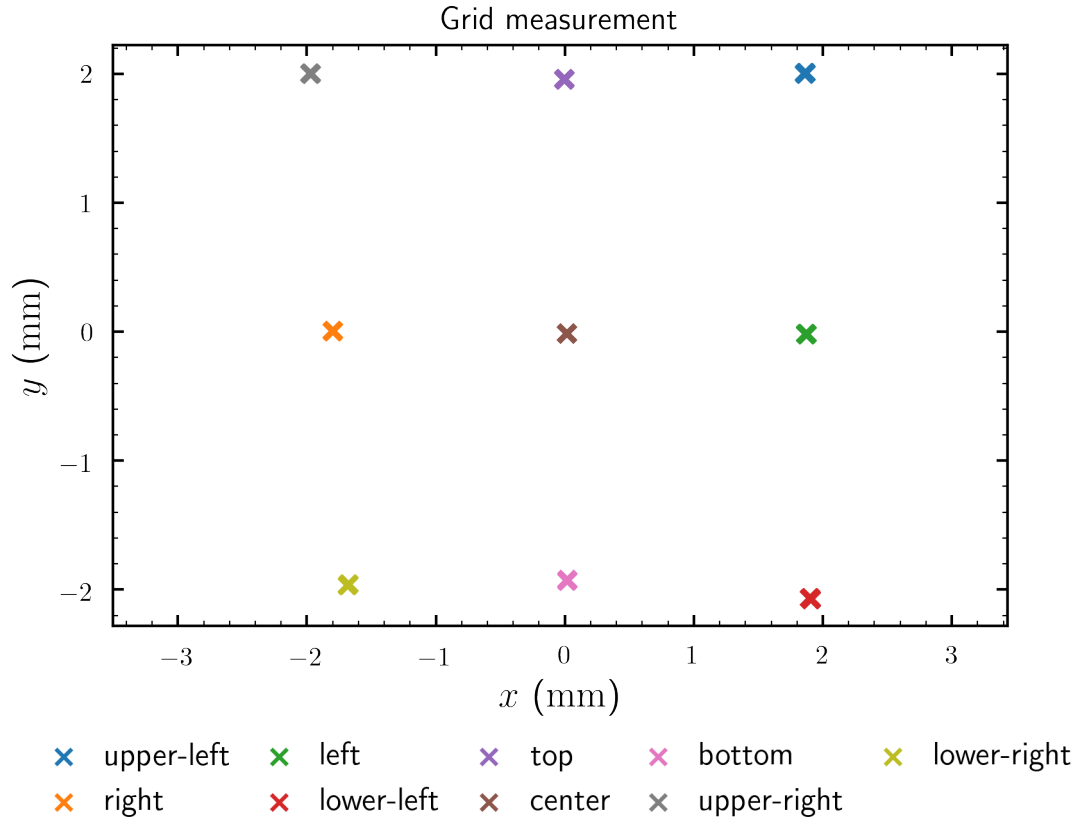Figure 26: Optical setup for testing

6.3. Grid scan

Figure 27: Spatial scan over 3×3 grid by adjusting the mirrors.

Figure 27 shows the positions of a 3 x 3 grid scan. We adjusted mirror M2 in the optical setup shown in fig. 26 and captured a trace with the oscilloscope. In the post-processing, we converted the captured voltages to positions. The datasheet of the S5990 position-sensitive photodiode gives a conversion formula for the photocurrents

$$\frac{(I_2 + I_3) - (I_1 + I_4)}{I_1 + I_2 + I_3 + I_4} = \frac{2x}{L}, \qquad \frac{(I_2 + I_4) - (I_1 + I_3)}{I_1 + I_2 + I_3 + I_4} = \frac{2y}{L}, \qquad (35)$$

wherein L is the length of the photodiode's quadratic sensitive area. In our case, we have the smaller S5991-01 photodiode where $L = 4\,\mathrm{mm}$. In terms of the output voltage signals of the PSD, the positions are then given by

$$x = \frac{L}{2}\frac{\mathrm{DIFFX}}{\mathrm{SUM}}\,\mathrm{mm}, \qquad\qquad y = \frac{L}{2}\frac{\mathrm{DIFFY}}{\mathrm{SUM}}\,\mathrm{mm}. \qquad (36)$$
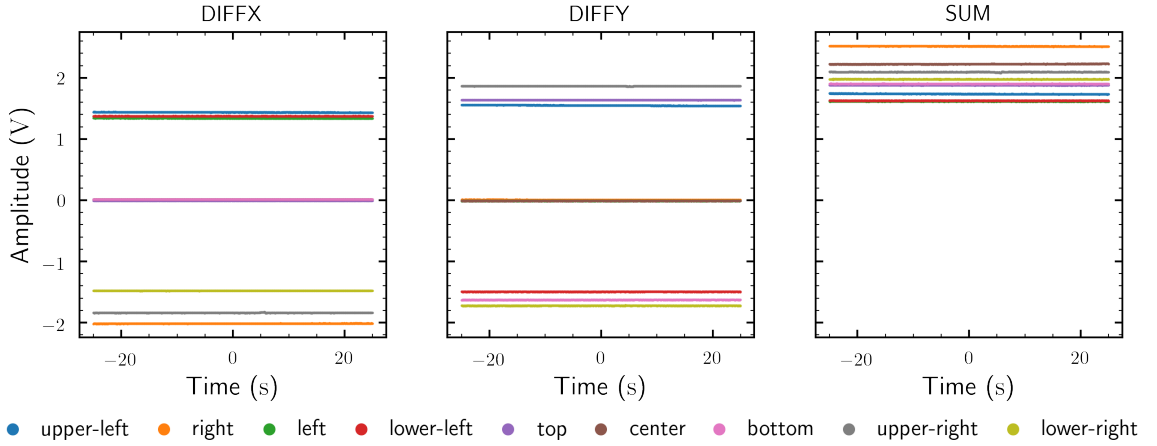
6.4. Resolution

Figure 28: Timeseries of the voltage signals captured during the grid scan.

Figure 28 shows the voltage signals for the grid scan measurement. The change of the SUM signal for the different measurements indicates a change in the total intensity of the detected light. We note that the difference signals span a voltage range from $-2\,\mathrm{V}$ to $2\,\mathrm{V}$.

Figure 29 shows the positions obtained from the voltages signals after using eq. (35). Horizontal and vertical axis span an area of close to $4\,\mathrm{mm}$ in agreement with the specified length of the sensitive area of the S5991-01. We explain small deviations by the fact that we cannot precisely control the mirror adjustments.

Table 2 summarizes the statistics, mean and standard deviation, of the position traces illustrated in fig. 29. For different grid positions, we find different positional uncertainty.
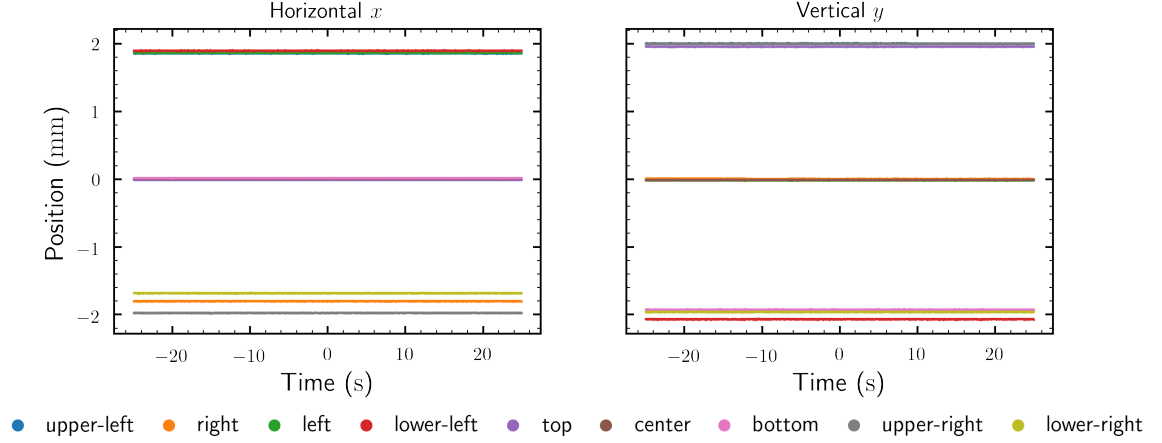
Figure 29: Voltage signals of the grid scan converted to positions.

The highest resolution with about $1\,\mu m$ is obtained close to the center. This is in agreement with our theoretical discussion of the position-sensitive photodiode designs where we claimed that non-linear effects become notable close to the border of the sensitive area.

Measurement	x (mm)	Δx (µm)	y (mm)	Δy (µm)
Center	0.01	1.08	−0.01	1.03
Top	−0.01	1.30	1.96	1.67
Left	1.87	2.19	−0.01	1.50
Right	−1.80	1.38	0.01	1.61
Bottom	0.02	1.24	−1.92	2.11
Upper left	1.86	2.03	2.01	2.50
Upper right	−1.97	1.75	2.00	1.65
Lower left	1.90	2.26	−2.07	2.56
Lower right	−1.68	1.78	−1.96	1.87

Table 2: Position statistics of 3×3 grid scan

6.5. Dark noise

For completeness, we performed a measurement of the detector where the sensitive area is blocked. Table 3 summarizes the statistics of the measurement. The variance of the voltage signals without illumination are much less than with illumination. It is difficult to distinguish the electronic from the detector noise.

Signal	Mean (mV)	Standard deviation (µm)
DIFFX	0.1	17
DIFFY	0.4	17
SUM	1.2	32

Table 3: Signal statistics obtained without illumination

6.6. Gaussian beam waist

Finally, we want to compare the focused beam waist to the positional uncertainty of table 2.

In Gaussian beam optics, we define the Rayleigh length

$$z_R = \frac{\pi w_0^2}{\lambda}. \tag{37}$$

Using a white paper, a pen, and a ruler, we estimated the spot size in front of the lens in fig. 26 to be less than $w_0 = 3\,\mathrm{mm}$. For simplicity, we assume $\lambda = 700\,\mathrm{nm}$ as the laser wavelength, and estimate the Rayleigh length to be $z_R = 40\,\mathrm{m}$.

Consider a Gaussian beam with initial beam waist w_0 and Rayleigh length z_R propagating through a thin lens with focal length f. After a distance of s, the beam waist of the Gaussian beam has the size

$$w_0' = \frac{w_0}{\sqrt{(1 - s/f)^2 + (z_R/f)^2}}. \tag{38}$$

For the optical setup given in fig. 26, $z_R = 40\,\mathrm{m}$, $w_0 = 3\,\mathrm{mm}$, $s = 11\,\mathrm{cm}$, $f = 50\,\mathrm{mm}$, eq. (38) yields $w_0' = 4\,\mathrm{\mu m}$. A beam waist of $4\,\mathrm{\mu m}$ is four times the estimated position uncertainty at the center of the PSD. We conclude that it is unlikely for the position uncertainty to be related to the spot size.

A. Troubleshooting

In this section, we record phenomena and their respective origin that we found during debugging[7].

A.1. Shorts

The most common sources for shorts we experienced originated from the soldering process. More precisely, this means displaced components and adverse solder joints. The best strategy to find shorts is by using a microscope and scrutinizing the solder points. If this doesn't help, one needs to remove components step-by-step. As we had most problems with capacitors, we recommend starting with the capacitors.

Alternative strategies for finding shorts include using an infrared (IR) camera to detect hot spots on the PCB. However, this won't work for shorts caused by unwanted solder. A very advanced technique measures the voltage drop across the components to narrow down the short. Consult your electrical engineer for details.

A.2. $50\,\mathrm{Hz}$ noise

$50\,\mathrm{Hz}$ noise is a characteristic of switching power supplies. We found that unisolated banana cables connected to a laboratory power supply act as an antenna. We highly recommend using isolated LEMO4 cables for power supply.

A.3. Power supply noise

When searching for noise sources, always check that the power supply provides clean voltages. More than once did we experience defect photodiode power supplies where this was not the case.

A.4. Unstable operational amplifiers

If the feedback capacitance is too small, operational amplifiers can become unstable. Unstable operational amplifiers behave as high-frequency oscillators. For more details on

---

[7]In the following, we use the term "noise" in the generic sense of (strong) unwanted signal instead of the strict statistical sense. Of course, random noise, e.g., thermal or shot noise, will always be present.

operational amplifier stability consult section 3.4. One can quickly check if an operational amplifier is a source for oscillations by grounding the input pins. Grounded input pins should yield a zero output voltage of the operational amplifier, i.e., make the oscillations vanish.

A.5. Malfunctioning capacitors

Broken capacitors are the most difficult to find troublemakers. We found one of them at the voltage regulator and another at the voltage reference. In both cases, the supply voltage was highly unstable and oscillating. We believe that using high-capacitance with a small casing size, e.g., 0603, increases the risk of malfunction. For this reason, we use large casing sizes, e.g., 1210, for high-capacitance capacitors in the recent design.

Glossary

BNC Bayonet Neill–Concelman. 34

BOM bill of materials. 29, 31

GBP gain-bandwidth-product. 23, 25

HTML hypertext markup language. 29–31

IC integrated circuit. 32

IR infrared. 39

PCB printed circuit board. 25, 29, 31, 39

PSD position-sensitive detector. 3, 34, 36, 38

S5990 Hamamatsu two-dimensional PSD. 12

SMA SubMiniature version A. 31, 34

SMD surface mounted device. 31

References

[1] Bruce Carter and Ron Mancini. *Op Amps for Everyone*. Elsevier, 2002. ISBN: 9780750677011.

[2] Tadayoshi Doke et al. "A new two-dimensional position sensitive detector with a good linear response". In: *Nuclear Instruments and Methods in Physics Research Section A: Accelerators, Spectrometers, Detectors and Associated Equipment* 261.3 (1987), pp. 605–609. DOI: 10.1016/0168-9002(87)90377-9.

[3] Jerald Graeme. *Photodiode Amplifiers. Op Amp Solutions*. McGraw Hill Professional, 1996. ISBN: 9780070242470.

[4] Philip Hobbs. *Building Electro-Optical Systems. Making it all Work*. John Wiley & Sons, 2011. ISBN: 9781118211090.

[5] Walt Jung. *Op Amp Applications Handbook*. Elsevier, 2005. ISBN: 9780750678445.

[6]   Art Kay. *Operational Amplifier Noise. Techniques and Tips for Analyzing and Reducing Noise*. Elsevier, 2012. ISBN: 9780750685252.

[7]   Anssi Mäkynen. "Position-sensitive devices and sensor systems for optical tracking and displacement sensing applications". PhD thesis. University of Oulu, 2000.

[8]   Date Noorlag. "Lateral-photoeffect position-sensitive detectors". PhD thesis. Delft University of Technology, 1974.

[9]   *S5990 2D PSD*. Hamamatsu. May 2013. URL: https://www.hamamatsu.com/resources/pdf/ssd/s5990-01_etc_kpsd1010e.pdf (visited on 03/03/2019).

[10] Walter Schottky. "Über den Entstehungsort der Photoelektronen in Kupfer-Kupferoxydul-Photozellen". In: *Zeitschrift für Physik* 31 (Nov. 1930), pp. 913–925.

[11] Steven H. Simon. *The Oxford Solid State Basics*. OUP Oxford, 2013. ISBN: 9780199680771.

[12] David Terrel. *Op Amps. Design, Applications, and Troubleshooting*. Butterworth-Heinemann, 1996. ISBN: 9780750697026.

[13] Ulrich Tietze, Christian Schenk, and Eberhard Gramm. *Electronic Circuits. Handbook for Design and Applications*. Springer, 2015. ISBN: 9783540786559.

[14] Gerald Wallmark. "Photoeffects in Nonuniformly Irradiated p-n Junctions". In: *Journal of Applied Physics* 31.6 (1960), pp. 1088–1085. DOI: 10.1063/1.1735750.

[15] J. T. Wallmark. "A New Semiconductor Photocell Using Lateral Photoeffect". In: *Proceedings of the IRE* 45.4 (Apr. 1957), pp. 474–483. DOI: 10.1109/JRPROC.1957.278435.

[16] Wanjun Wang and Ilene Busch-Vishniac. "The linearity and sensitivity of lateral effect position sensitive devices-an improved geometry". In: *IEEE Transactions on Electron Devices* 261.11 (Nov. 1989), pp. 2475–2480. DOI: 10.1109/16.43670.

[17] Hermann Woltring. "Single- and dual-axis lateral photodetectors of rectangular shape". In: *IEEE Transactions on Electron Devices* 22.8 (Aug. 1975), pp. 581–590. DOI: 10.1109/T-ED.1975.18181.